Reduction of Cross-Beam Energy Transfer by a Speckle Pattern

A. Oudin,* A. Debayle,† C. Ruyer, and D. Bénisti
CEA, DAM, DIF, F-91297 Arpajon, France
and Université Paris-Saclay, CEA, LMCE, 91680 Bruyères-le-Châtel, France

(Received 19 July 2021; revised 26 October 2021; accepted 30 November 2021; published 23 December 2021)

In this Letter, we show that cross-beam energy transfer (CBET), ubiquitous in inertial confinement fusion (ICF) experiments, may be strongly modified by the speckle pattern of the beams. This is demonstrated by the means of two-dimensional particle in cell simulations, supported by a linear model. In particular, we show that, although they would be the same in a plane wave model, the exchange rates of energy may be significantly different whether there is a plasma flow, or a wavelength shift, especially when the waves are weakly damped. When the crossed laser beams have different frequencies, the energy exchange rate is substantially reduced compared with the predictions of the plane wave model, widely used in the hydrodynamic codes that model and interpret ICF experiments. Such effects can partly explain the disagreement of the CBET predictions compared with experimental results.

DOI: 10.1103/PhysRevLett.127.265001

Achieving inertial confinement fusion (ICF) requires the highly symmetric compression of a deuterium-tritium shell [1–4] by the means of more than one hundred laser beams. In the direct drive scheme, the target implosion is driven by the laser-assisted capsule shell ablation. In the indirect drive scheme, the laser beams are focused inside a gold hohlraum to convert the monochromatic light into an x-ray thermal bath. Then, the capsule located in the hohlraum center is imploded due to the shell ablation by the x radiation. In both schemes, there is an energy exchange between the overlapping beams, known as cross-beam energy transfer (CBET). The energy goes from the blue-shifted laser beams, in the plasma reference frame, to the red-shifted laser beams. The energy exchange is significant [5–10] and affects the homogeneity of energy deposition in both direct and indirect drive schemes [11–13]. It is used to balance the amount of power between the laser cones at national ignition facility (NIF) [14–16] in order to improve the symmetry of the target implosion. This is achieved by tuning the beams wavelengths so as to induce CBET from the outer (50° and 44.5°) to the inner (30° and 23.5°) cones. Significant efforts [17–22] have been made to include CBET in the hydrodynamic modeling of ICF experiments. Based on the locally homogeneous steady-state linear plane wave approximation (that will henceforth be simply called "plane wave approximation"), these models neglect the speckle structure of the spatially smoothed laser beams. As further discussed in this Letter, this oversimplification may explain the difficulties of reproducing the experimental results.

CBET is a three-wave mixing process which occurs when two coherent laser beams cross each other, leading to an interference pattern in the crossing region. Electrons are pushed away from the strong field region by the ponderomotive force, and are followed by ions due to the electrostatic potential. An ionic acoustic wave (IAW) is formed, partially scattering one beam along the direction of the second beam thereby producing an energy exchange. Let ω_0 and ω_1 be the laser wave frequencies, and $\mathbf{k}_0$ and $\mathbf{k}_1$ be their wave numbers. Because the IAW results from the beating of the two lasers, its wave number is $\mathbf{k} = \mathbf{k}_0 - \mathbf{k}_1$, and its frequency is $\omega = \omega_0 - \omega_1 - \mathbf{k}\cdot\mathbf{v}_d$, where $\mathbf{v}_d$ is the plasma flow velocity. CBET is most effective when the IAW is excited at resonance, i.e., when $\omega = kc_s = |\mathbf{k}|c_s$, where c_s is the sound speed. Hence, the phase matching condition for CBET reads as $\omega_0 - \omega_1 - (\mathbf{k}_0 - \mathbf{k}_1)\cdot\mathbf{v}_d = (k_0 - k_1)c_s$.

Within the plane wave approximation, equal frequency laser beams crossing in a sonic plasma ($\mathbf{k}\cdot\mathbf{v}_d/k = -c_s$) exchange the same amount of energy as two laser beams with frequency difference $\omega_0 - \omega_1 = (k_0 - k_1)c_s$, in a plasma with no flow. Nevertheless, there is an inherent difference between these two configurations. In the reference frame of a moving plasma, the envelope of two crossing speckles, together with the interference grating, are moving at $\mathbf{v}_d$. In a stationary plasma, the wavelengths' shift leads to an interference grating moving at $\omega/|\mathbf{k}|$ whereas the speckle crossing envelope remains motionless. For infinite laser envelope or when the Landau damping distance is small compared with the speckle waist, both situations become equivalent. Yet, in most ICF plasmas, these two systems are distinct because the IAWs are not stimulated by the same potential well. In the present Letter, we demonstrate that the speckle structure questions the relevance of the plane wave approximation in the wavelength shift case, and can explain the disagreement between models and experimental results involving mid to high Z materials, before accounting for ion trapping [23–25] or

beam deflection and self-focusing [26]. The speckle structure may reduce CBET by about 10% in strongly damped plastic CH plasmas, and up to 50–70% in high Z silicon ablators [27] or in the gold bubble in low gas filled hohlraum [13].

We first present 2D Calder [28] particle-in-cell simulations describing the exchange between two beams, each composed of four speckles in a weakly damped plasma. We consider situations with and without plasma flow, and when CBET is at, or out of, resonance. Moreover, a linear model is introduced to support our simulation results and to estimate the plasma parameters for which the speckle structure cannot be neglected.

Figure 1(a) illustrates the simulations setup, consisting of two beams, each composed of four speckles, crossing each other. Compared to real spatially smoothed beams, this simplified configuration allows one to compare the results with the plane wave case while having a perfect knowledge of the intensities and the phase shifts between the waves. The laser pulses propagate from the left to the right. The temporal evolution is a ramp of $1000\omega_0^{-1}$ followed by a plateau until the end of the simulation. The focal spots of the eight speckles are located in the middle of the simulation box, and their intensity is $I = 8.8 \times 10^{13}\,\mathrm{W\,cm^{-2}}$ with equal beam waists at $1/e$, $w = 70\ c\omega_0^{-1}$ (11 μm for a laser wavelength of $\lambda = 1$ μm). All speckles are equally spaced by $\Delta y = 150\ c\omega_0^{-1}$. In the following, each group of four speckles is referred to as a beam. The frequency shift is either chosen so as to match the resonance condition $\omega = kc_s = 1.8 \times 10^{-4}\omega_0$, or slightly away from the resonance, the lower beams having the lowest frequency. In order to obtain a small damping without numerical heating, the plasma is composed of ions with a fixed ionization state $Z = 10$ and an atomic number of $A = 160$. The electron-ion temperatures are $T_e = 4$ keV, $T_i = 1$ keV. The resulting damping distance is $c_s/\nu \approx 700 c\omega_0^{-1}$ which is twice the value of the distance for a gold plasma. The electron density, normalized to the laser critical density, is $n_{e_0} = 0.04$. Moreover, we used an alternating-order interpolation scheme [29] at fourth order, together with a high mode current filtering. The ion and electron heating, for all simulations, are below 10% over 1.2 million time steps, which corresponds to a physical time of 190 ps for $\lambda = 1\,\mu$m.

Figure 1 plots the normalized profile of the laser intensity, and of the electron density perturbation $\delta N_e/n_{e0}$, along y. In a stationary plasma with a wavelength shift [Fig. 1(b)], the propagating IAWs are clearly visible and have time to reach the next crossing regions due to the small damping rate. When there is a plasma flow, but no frequency shift, the IAWs are stationary in the lab frame, as shown in Fig. 1(c). The amplitude of the density perturbation is weaker when the plasma is stationary, because the propagating wave does not have the time to locally grow. Moreover, the phase shift between waves created in the vicinity of different crossing regions may decrease the total IAW amplitude, exacerbating the disparities with the plasma flow case. From these different IAW amplitudes, we anticipate a substantial difference in the energy exchange. We checked this numerically by performing several simulations, with or without plasma flow, and with various phase shifts between the speckles. Because the waves are weakly damped, we could not reach the asymptotic regime in our simulations.

Figure 2(a) compares the gain-loss of linear power of the upper-lower escaping beams for different laser and plasma parameters. The red diamonds correspond to a temporal plane wave model inspired from Ref. [30] and show a satisfying correspondence with the plasma flow case. At resonance, the exchange in energy is 20% larger when there is a plasma flow case (dotted line) than when there is a wavelength shift case (dashed-dotted line). This difference is further increased beyond 100% by adding a phase shift between the speckles (dashed line). It is worth pointing out that the upper beam is significantly depleted in the plasma flow case, thereby limiting the inner beam's power growth. For smaller intensities, the disparities between the three cases would be even more pronounced. Despite this intrinsic difference in the IAW growth shown in Fig. 1, the energy exchange due to a plasma flow can be canceled out

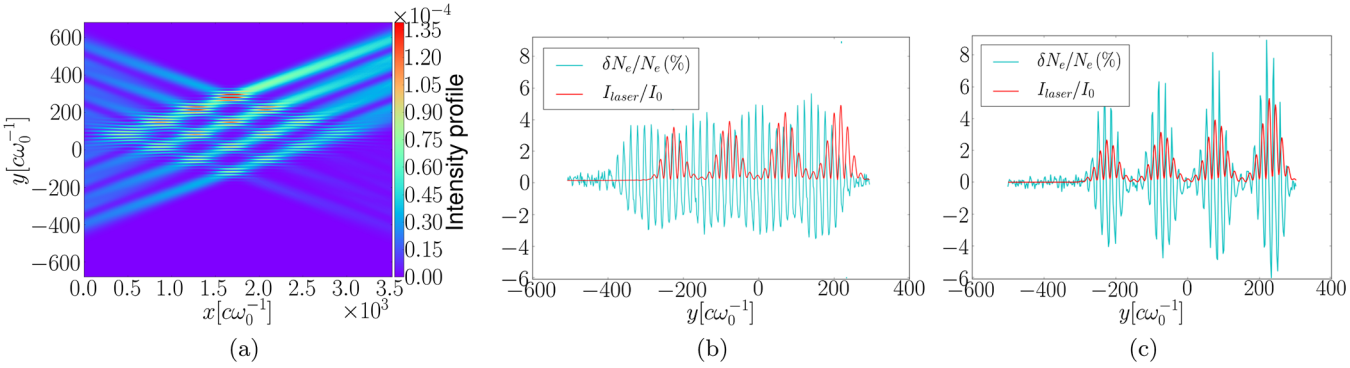

FIG. 1. (a) Intensity profile normalized to $2.74 \times 10^{18}/(\lambda/[1\ \mu\mathrm{m}])^2\ \mathrm{W\,cm^{-2}}$ at time $3.4 \times 10^5 \omega_0^{-1}$ for the plasma flow case. (b) and (c) Percentage of electronic wave perturbation (cyan) and normalized laser intensity (red) as a function of y and averaged from $x = 1600$ to $x = 1800 c\omega_0^{-1}$ in the laboratory frame at $t = 2.71 \times 10^5 \omega_0^{-1}$ for the wavelength shift case (a), and for the plasma flow case (b).

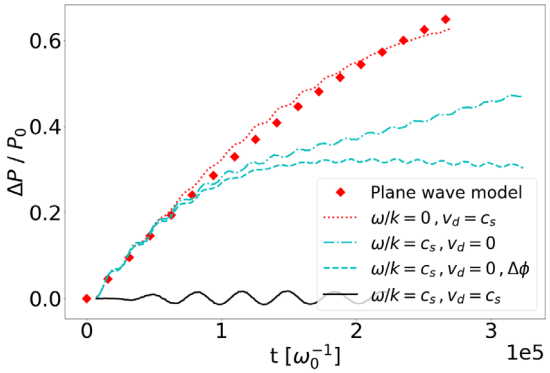

(a)

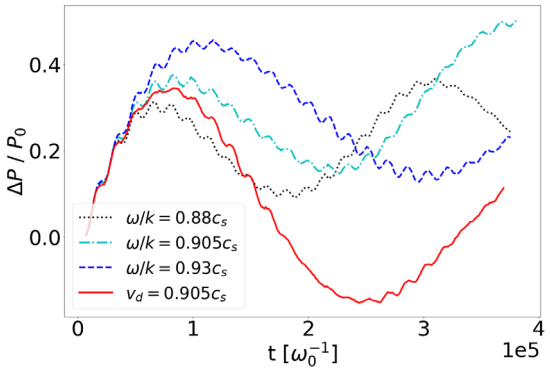

(b)

FIG. 2. Difference between the linear power of the upper and the lower beam versus time. (a) At resonance for the plasma flow case in red (dotted line), the wavelength shift case in cyan, with (dashed lines) and without (dashed-dotted line) phase shift, and out of resonance in black (plane line). (b) Out of resonance for the plasma flow case (plane red line) and for the wavelength shift case for three values of ω/k corresponding to three different resonance deviations in cyan, blue, and black.

by adding a frequency shift ($\omega/k = c_s$ and $v_d = c_s$) as illustrated by the black curve in Fig. 2(a). Indeed, out of resonance the IAW amplitude is very small.

To study the resonance bandwidth, the exchanged power is plotted in Fig. 2(b) for one out-of-resonance plasma flow case, and three values of ω/k for the wavelength shift case. For a flow velocity, $v_d = 0.905c_s$, the transient exchange oscillates around zero, before vanishing at long times, in a similar way as in Fig. 2(a) of Ref. [30]. As explained subsequently by the linear model, the solution behaves like in the plane wave case, for which the resonance bandwidth of the weakly damped plasma is thin. By contrast, the exchange persists in the wavelength shift case. The different values of ω/kc_s (0.88, 0.905, and 0.93) are chosen so as to explore the resonance bandwidth. The comparable amount of power exchange in the three cases suggests a larger resonance bandwidth than in the plasma flow case. This peculiar tendency can be explained by our model.

The effect of the speckles envelope on the energy exchange may be deduced from the electron density perturbation, in the plasma reference frame. Let $\mathbf{v}_{d_\parallel}$ be the plasma flow velocity along $\mathbf{k}$, assumed to be in the $\hat{\mathbf{y}}$ direction. From the model presented in [30], δN_e solves

$$[(\partial_t + v_{d_\parallel}\partial_y)^2 + 2\nu(\partial_t + v_{d_\parallel}\partial_y) - c_s^2\partial_y^2]\delta N_e = \frac{\alpha}{2}(\cos k_{\rm sp} y + 1)e^{i(ky-\omega t)}e^{i\phi}, \tag{1}$$

where $\alpha = [(Z^2 n_{i,0}|\boldsymbol{k}|^2)/4\tilde{m}_i]a_0 a_1$, $\tilde{m}_i$ is the ion mass normalized to the electron mass, $n_{i,0}$ is the unperturbed ion density normalized to the critical density, Z is the atomic number, and a_0, a_1 are the vector potential amplitudes of the two crossing speckles, normalized to $m_e c/e$. In the most general situation, ν is the sum of the Landau and electron-ion collisional [31] damping rates. The equation is solved for a coexisting plasma flow and wavelength shift, which enables one subsequently to choose $\omega = 0$ or $v_{d_\parallel} = 0$. The constructive-destructive interference between the interacting waves is modeled by adding a continuous phase shift to the envelop

$$e^{i\phi} = e^{i\pi \sin\beta y} = \sum_{n\in\mathbb{Z}} J_n(\pi)e^{in\beta y}, \tag{2}$$

allowing one to obtain a different phase for each crossing speckle. The linearized ion acoustic wave described by Eq. (1) is driven by a grating, of wave number $\mathbf{k}$, modulated by an oscillating envelope of wave vector $k_{\rm sp}$, so as to model a juxtaposition of crossing speckles. Thus, the interspeckle distance is $\lambda_{\rm sp} = 2\pi/k_{\rm sp}$, and the phase shift between two neighboring crossing speckles is controlled by fixing $\beta = 0$ (in phase) or $\beta \in]0; k_{\rm sp}/12]$ (out of phase). In the asymptotic limit ($\nu t \gg 1$), the driven solution is

$$\delta N_e^{\rm driven} = \frac{\alpha}{2}e^{iky-i\omega t}\sum_{n\in\mathbb{Z}} J_n(\pi)e^{in\beta y} \times \left[\tilde{f}(k+n\beta) + \frac{1}{2}\tilde{f}(k+k_{\rm sp}+n\beta)e^{ik_{\rm sp}y} + \frac{1}{2}\tilde{f}(k-k_{\rm sp}+n\beta)e^{-ik_{\rm sp}y}\right], \tag{3}$$

with

$$\tilde{f}(k) = \frac{1}{-(kv_{d_\parallel}-\omega)^2 + 2i\nu(kv_{d_\parallel}-\omega) + c_s^2k^2}, \tag{4}$$

where $\tilde{f}(k)$ is the driven acoustic wave envelope of a plane wave of wave number k and frequency ω. The power exchange induced by the driven acoustic wave is ruled by the wave coupling equations

$$2i\boldsymbol{k_0}\cdot\boldsymbol{\nabla}A_0 = \delta N_e^{\rm driven}A_1 e^{-i\boldsymbol{k}\cdot\boldsymbol{r}+i\omega t}, \tag{5}$$

$$2i\boldsymbol{k_1}\cdot\boldsymbol{\nabla}A_1 = \delta N_e^{\star\,\rm driven}A_0 e^{i\boldsymbol{k}\cdot\boldsymbol{r}-i\omega t}, \tag{6}$$

where $A_{0,1}(\mathbf{r})$ are the vector potential envelopes of the laser beams. In the perturbation limit, Eq. (5) becomes

$$\boldsymbol{k_0}\boldsymbol{\nabla}\delta I_0 = \frac{a_0 a_1}{2}(\cos k_{\rm sp} y + 1)\mathrm{Im}\{\delta N_e^{\rm driven}\}, \qquad (7)$$

where $A_0 A_1^\star \approx a_0 a_1(\cos k_{\rm sp} y + 1)/2$. As $\mathbf{k}_0\cdot\nabla = k_0\cos\theta\partial_x + k_0\sin\theta\partial_y$, the solution after a propagation length of $\lambda_{\rm sp}/\sin\theta$ is

$$\frac{\delta I_0}{I_0} = \frac{\lambda_{\rm sp}}{k_0\sin\theta}\overline{\delta N_e}^{\rm driven}, \qquad (8)$$

where $\overline{\delta N_e}^{\rm driven}$ is the mean value along y (and β for the phase shift case), and $I_0 = a_0^2/2$. Figure 3(a) plots $\delta I_0/I_0$ [Eq. (8)] as a function of the normalized acoustic damping rate, for the plasma flow and the wavelength shift cases, with and without phase shift. The laser amplitudes, angles

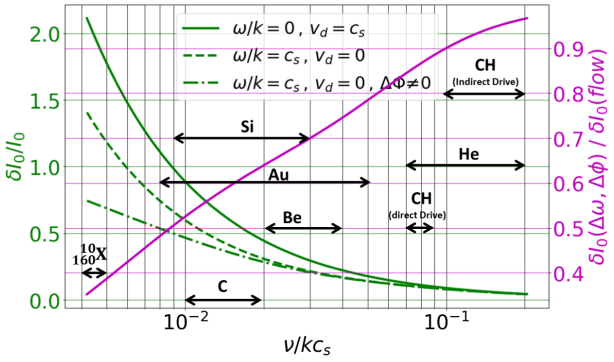

(a)

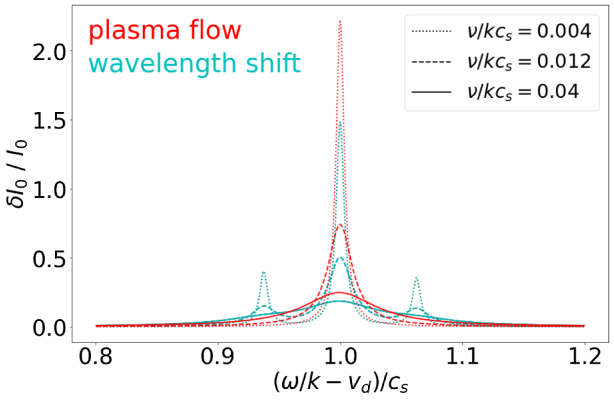

(b)

FIG. 3. (a) Semi-log plots of $\delta I_0/I_0$ versus the normalized acoustic wave Landau damping rate, at resonance $v_d = c_s$ (plane line) or $\omega = kc_s$ with (dashed-dotted lines) and without (dashed line) phase shift. The parameters are $k_{sp} = 0.0625k$, ν varies between 0.0041ω and 0.2ω. The magenta curve is the ratio between the wavelength and phase shift case and the plane wave case. (b) Amplitude of $\delta I_0/I_0$ versus the deviation to resonance for three damping values for plasma flow case (red curves) and wavelength shift cases (cyan curves).

and the plasma density and temperatures match those of the simulations. The damping is varied to illustrate the different interaction regimes. The smallest damping value corresponds to the plasma used in the (collisionless) simulation ($A = 160$, $Z = 10$). There, the parameter $\nu/kc_s = 4\times10^{-3}$ corresponds to a Landau damping distance 10 times greater than the speckle's size $\lambda_{\rm sp}$. The order of magnitude of this parameter is indicated for a few plasmas relevant to ICF: the gold bubble of indirect drive configuration, the indirect drive CH with NIF parameters, the direct drive CH with omega parameters (CH_4 giving the same value), carbon, helium, and the higher Z ablators silicon and beryllium [27,32]. These calculations are made assuming temperatures ranging from $T_e \sim 2T_i = 1$–4 keV and densities around $n_{e0} = 0.01$–0.1. Concerning the high Z plasmas, the range of the damping rates includes the effect of electron-ion collision, based on Ref. [31]. For Au (Si), the plasma collisionality may increase the damping rate up to ~0.05 (~0.03) depending on the cone angle and local plasma parameters. As the model does not take into account the depletion of the beam, $\delta I_0/I_0$ reaches very high values (> 1) but the different tendencies of these three cases corroborate the simulation results. In the weakly damped regime—corresponding to the simulations denoted by X—for the gold or the silicon, a greater exchange rate is observed with a plasma flow, while the smallest exchange is obtained with a wavelength shift and out of phase crossed speckles. Because the damping distance is greater than the distance between the crossed speckles, the driven wave with a frequency shift is substantially reduced due to destructive interferences. In contrast, the power exchange in the plasma flow case without frequency shift closely corresponds to the plane wave model, i.e., $\delta N_e^{\rm driven} \approx \alpha/2e^{iky-i\omega t}\tilde{f}(k)$. For intermediate damping rates, as for the carbon, helium, and beryllium plasmas, the difference between both wavelength shift cases fades away as the IAW is damped before reaching another crossing. However, a large difference remains between the wavelength shift and plasma flow cases. As the damping distance is comparable to the speckle size, the driven IAW differs from the plane wave case. For strong damping rates, as for the CH plasmas, a difference of ≈10% (indirect drive) and 20% (direct drive) remains. For very large damping rates (> 0.2), all considered situations become equivalent, hence demonstrating the validity of the plane wave approximation. Further, the broadening of the resonance bandwidth evidenced by our simulation results [see Fig. 2(b)] is also explained by our linear model. Figure 3(b) illustrates the dependence of $\delta I_0/I_0$ on $(\omega/k - v_d)/c_s$ for three damping values, either in the case of a plasma flow (cyan) or a wavelength shift (red). The amplitudes at resonance are the same as in Fig. 3(a), yet, for the wavelength shift case, two more peaks are located at $\omega/(k + k_{\rm sp}) = c_s$ and $\omega/(k - k_{\rm sp}) = c_s$. These resonances, amplified by the periodicity of our model, is due to the beating between

the IAW induced by the grating k and the IAWs induced by the speckle's envelope $\pm k_{sp}$. For realistic spatially smoothed laser beams, the randomness of the speckle's position involves a wide range of wave vectors, and should result in a broadening of the resonance bandwidth, instead of two additional peaks.

In conclusion, using both numerical simulations and an analytical model, we investigated the energy exchange between laser beams, which either had shifted wavelengths in a stationary plasma, or the same frequency in a drifting plasma. We showed that the energy rate was significantly smaller in the first situation than in the second one, all the more so as the IAWs were weakly damped. This strong inhibition is due to the destructive interference between the many IAWs produced by the gratings. This lets us conclude that the plane wave models of CBET, used in ICF hydrodynamic codes, tend to overestimate the energy exchange because it cannot account for the speckle-induced IAW interferences. However, we also conclude that plane wave models should correctly capture the linear CBET regime when the laser frequencies are the same.

We acknowledge important input from X. Davoine and G. Sary. This work has been done under the auspices of Commissariat à l'Energie Atomique (CEA), and the simulations were performed using high performance computing resources at Centre de Calcul pour la Recherche et la Technologie and CEA/Tera.

*albertine.oudin@cea.fr
†arnaud.debayle@cea.fr

[1] J. Nuckolls, L. Wood, A. Thiessen, and G. Zimmerman, Laser compression of matter to super-high densities: Thermonuclear (CTR) applications, Nature (London) **239**, 139 (1972).

[2] C. Cavailler, Inertial fusion with the LMJ, Plasma Phys. Controlled Fusion **47**, B389 (2005).

[3] J. D. Lindl, P. Amendt, R. L. Berger, S. G. Glendinning, S. H. Glenzer, S. W. Haan, R. L. Kauffman, O. L. Landen, and L. J. Suter, The physics basis for ignition using indirect-drive targets on the national ignition facility, Phys. Plasmas **11**, 339 (2004).

[4] W. Zheng *et al.*, Laser performance upgrade for precise ICF experiment in SG-III laser facility, Matter Radiat. Extremes **2**, 243 (2017).

[5] B. L. Stansfield, R. Nodwell, and J. Meyer, Enhanced Scattering of Laser Light by Optical Mixing in a Plasma, Phys. Rev. Lett. **26**, 1219 (1971).

[6] R. K. Kirkwood, B. B. Afeyan, W. L. Kruer, B. J. MacGowan, J. D. Moody, D. S. Montgomery, D. M. Pennington, T. L. Weiland, and S. C. Wilks, Observation of Energy Transfer between Frequency-Mismatched Laser Beams in a Large-Scale Plasma, Phys. Rev. Lett. **76**, 2065 (1996).

[7] K. B. Wharton, R. K. Kirkwood, S. H. Glenzer, K. G. Estabrook, B. B. Afeyan, B. I. Cohen, J. D. Moody, and C. Joshi, Observation of Energy Transfer between Identical-Frequency Laser Beams in a Flowing Plasma, Phys. Rev. Lett. **81**, 2248 (1998).

[8] P. Zhang, N. Saleh, S. Chen, Z. M. Sheng, and D. Umstadter, Laser-Energy Transfer and Enhancement of Plasma Waves and Electron Beams by Interfering High-Intensity Laser Pulses, Phys. Rev. Lett. **91**, 225001 (2003).

[9] C. Neuville, C. Baccou, A. Debayle, P. E. Masson-Laborde, S. Hüller, M. Casanova, D. Marion, P. Loiseau, K. Glize, C. Labaune, and S. Depierreux, Spatial and Transient Effects during the Amplification of a Picosecond Pulse Beam by a Nanosecond Pump, Phys. Rev. Lett. **117**, 145001 (2016).

[10] C. Neuville, K. Glize, P.-E. Masson-Laborde, P. Loiseau, S. Hüller, A. Debayle, C. Baccou, M. Casanova, C. Labaune, and S. Depierreux, Polarization modification of a spatially randomized picosecond-pulse beam during its amplification by a nanosecond pump, Phys. Plasmas **24**, 112110 (2017).

[11] I. V. Igumenshchev, D. H. Edgell, V. N. Goncharov, J. A. Delettrez, A. V. Maximov, J. F. Myatt, W. Seka, A. Shvydky, S. Skupsky, and C. Stoeckl, Crossed-beam energy transfer in implosion experiments on omega, Phys. Plasmas **17**, 122708 (2010).

[12] I. V. Igumenshchev *et al.*, Crossed-beam energy transfer in direct-drive implosions, Phys. Plasmas **19**, 056314 (2012).

[13] A. L. Kritcher, J. Ralph, D. E. Hinkel, T. Döppner, M. Millot, D. Mariscal, R. Benedetti, D. J. Strozzi, T. Chapman, C. Goyon, B. MacGowan, P. Michel, D. A. Callahan, and O. A. Hurricane, Energy transfer between lasers in low-gas-fill-density hohlraums, Phys. Rev. E **98**, 053206 (2018).

[14] P. Michel, S. H. Glenzer, L. Divol, D. K. Bradley, D. Callahan, S. Dixit, S. Glenn, D. Hinkel, R. K. Kirkwood, J. L. Kline, W. L. Kruer, G. A. Kyrala, S. Le Pape, N. B. Meezan, R. Town, K. Widmann, E. A. Williams, B. J. MacGowan, J. Lindl, and L. J. Suter, Symmetry tuning via controlled crossed-beam energy transfer on the national ignition facility, Phys. Plasmas **17**, 056305 (2010).

[15] L. A. Pickworth *et al.*, Application of cross-beam energy transfer to control drive symmetry in icf implosions in low gas fill hohlraums at the national ignition facility, Phys. Plasmas **27**, 102702 (2020).

[16] D. H. Edgell, R. K. Follett, I. V. Igumenshchev, J. F. Myatt, J. G. Shaw, and D. H. Froula, Mitigation of cross-beam energy transfer in symmetric implosions on omega using wavelength detuning, Phys. Plasmas **24**, 062706 (2017).

[17] A. Colaïtis, G. Duchateau, X. Ribeyre, and V. Tikhonchuk, Modeling of the cross-beam energy transfer with realistic inertial-confinement-fusion beams in a large-scale hydrocode, Phys. Rev. E **91**, 013102 (2015).

[18] A. K. Davis, D. Cao, D. T. Michel, M. Hohenberger, D. H. Edgell, R. Epstein, V. N. Goncharov, S. X. Hu, I. V. Igumenshchev, J. A. Marozas, A. V. Maximov, J. F. Myatt, P. B. Radha, S. P. Regan, T. C. Sangster, and D. H. Froula, Isolating and quantifying cross-beam energy transfer in direct-drive implosions on omega and the national ignition facility, Phys. Plasmas **23**, 056306 (2016).

[19] L. Hao, X. Y. Hu, C. Y. Zheng, B. Li, J. Xiang, and Z. J. Liu, Study of crossed-beam energy transfer process with large crossing angle in three-dimension, Laser Part. Beams **34**, 270 (2016).

[20] D. J. Strozzi, D. S. Bailey, P. Michel, L. Divol, S. M. Sepke, G. D. Kerbel, C. A. Thomas, J. E. Ralph, J. D. Moody, and M. B. Schneider, Interplay of Laser-Plasma Interactions and Inertial Fusion Hydrodynamics, Phys. Rev. Lett. **118**, 025002 (2017).

[21] R. K. Follett, J. G. Shaw, J. F. Myatt, V. N. Goncharov, D. H. Edgell, D. H. Froula, and J. P. Palastro, Ray-based modeling of cross-beam energy transfer at caustics, Phys. Rev. E **98**, 043202 (2018).

[22] A. Debayle, C. Ruyer, O. Morice, P.-E. Masson-Laborde, P. Loiseau, and D. Benisti, A unified modeling of wave mixing processes with the ray tracing method, Phys. Plasmas **26**, 092705 (2019).

[23] P. Michel, W. Rozmus, E. A. Williams, L. Divol, R. L. Berger, R. P. J. Town, S. H. Glenzer, and D. A. Callahan, Stochastic Ion Heating from Many Overlapping Laser Beams in Fusion Plasmas, Phys. Rev. Lett. **109**, 195004 (2012).

[24] L. Yin, B. J. Albright, D. J. Stark, W. D. Nystrom, R. F. Bird, and K. J. Bowers, Saturation of cross-beam energy transfer for multispeckled laser beams involving both ion and electron dynamics, Phys. Plasmas **26**, 082708 (2019).

[25] A. M. Hansen, K. L. Nguyen, D. Turnbull, B. J. Albright, R. K. Follett, R. Huff, J. Katz, D. Mastrosimone, A. L. Milder, L. Yin, J. P. Palastro, and D. H. Froula, Cross-Beam Energy Transfer Saturation by Ion Heating, Phys. Rev. Lett. **126**, 075002 (2021).

[26] G. Raj and S. Hüller, Impact of Laser Beam Speckle Structure on Crossed Beam Energy Transfer via Beam Deflections and Ponderomotive Self-Focusing, Phys. Rev. Lett. **118**, 055002 (2017).

[27] V. N. Goncharov *et al.*, Improving the hot-spot pressure and demonstrating ignition hydrodynamic equivalence in cryogenic deuterium-tritium implosions on omega, Phys. Plasmas **21**, 056315 (2014).

[28] E. Lefebvre, N. Cochet, S. Fritzler, V. Malka, m.-m. Aleonard, J. Chemin, S. Darbon, L. Disdier, J. Faure, A. Fedotoff, O. Landoas, G. Malka, V. Meot, P. Morel, M. Rabec Le Gloahec, A. Rouyer, C. Rubbelynck, V. Tikhonchuk, R. Wrobel, and C. Rousseaux, Electron and photon production from relativistic laser-plasma interactions, Nucl. Fusion **43**, 629 (2003).

[29] I. V. Sokolov, Alternating-order interpolation in a charge-conserving scheme for particle-in-cell simulations, Comput. Phys. Commun. **184**, 320 (2013).

[30] A. Debayle, P. E. Masson-Laborde, C. Ruyer, M. Casanova, and P. Loiseau, Cross-beam energy transfer: On the accuracy of linear stationary models in the linear kinetic regime, Phys. Plasmas **25**, 052702 (2018).

[31] E. M. Epperlein, Effect of electron collisions on ion-acoustic waves and heat flow, Phys. Plasmas **1**, 109 (1994).

[32] R. K. Follett, J. A. Delettrez, D. H. Edgell, V. N. Goncharov, R. J. Henchen, J. Katz, D. T. Michel, J. F. Myatt, J. Shaw, A. A. Solodov, C. Stoeckl, B. Yaakobi, and D. H. Froula, Two-Plasmon Decay Mitigation in Direct-Drive Inertial-Confinement-Fusion Experiments using Multilayer Targets, Phys. Rev. Lett. **116**, 155002 (2016).